JACS
JOURNAL OF THE AMERICAN CHEMICAL SOCIETY
Article
pubs.acs.org/JACS

Probing the Free Energy Landscape of the Fast-Folding gpW Protein by Relaxation Dispersion NMR

Celia Sanchez-Medina,[†] Ashok Sekhar,[‡] Pramodh Vallurupalli,[‡] Michele Cerminara,[†] Victor Muñoz,*[,†] and Lewis E. Kay*[,‡,§]

[†]Centro de Nacional de Biotecnología, Consejo Superior de Investigaciones Científicas, Darwin 3, Campus de Cantoblanco, 28049 Madrid, Spain

[‡]Departments of Molecular Genetics, Biochemistry, and Chemistry, The University of Toronto, Toronto, Ontario, Canada M5S 1A8

[§]Program in Molecular Structure and Function, Hospital for Sick Children, 555 University Avenue, Toronto, Ontario, Canada M5G 1X8

Supporting Information

ABSTRACT: The topographic features of the free energy landscapes that govern the thermodynamics and kinetics of conformational transitions in proteins, which in turn are integral for function, are not well understood. This reflects the experimental challenges associated with characterizing these multidimensional surfaces, even for small proteins. Here we focus on a 62-residue protein, gpW, that folds very rapidly into a native structure with an α/β topology in which α-helices are at the N- and C-terminal ends of the molecule with a central β-hairpin positioned orthogonally to the helices. Using relaxation dispersion NMR spectroscopy to probe the conformational fluctuations in gpW at 1 °C, we found that the native state interconverts with a transiently formed, sparsely populated second state with a lifetime of 250 μs, consistent with the global folding−unfolding rate under these conditions. In this low-populated state, the β-hairpin is unfolded whereas the α-helices remain predominantly formed. Our results argue for a hierarchical stability of secondary structural elements and demonstrate the existence of a complex free energy landscape even in this small, fast-folding single-domain protein.

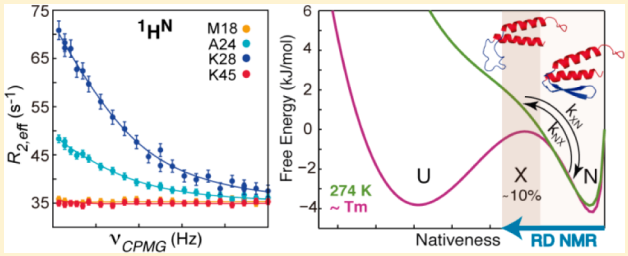

INTRODUCTION

Conformational fluctuations direct the folding of proteins into complex, functional, three-dimensional structures and often play important roles in molecular recognition and enzyme catalysis.[1] Conformational changes are usually described in terms of diffusive motions of protein molecules on a free energy surface of reduced dimensionality.[2,3] Minima on this landscape correspond to conformational ensembles whose relative free energies determine their populations, whereas barriers separating the states and the intramolecular diffusion coefficient establish the rates of their interconversion. Experimental characterization of the conformational free energy surface has proven to be difficult because of its underlying complexity, and several aspects, including the magnitudes of the free energy barriers separating states, the barrier transition paths, and the identification and structural elucidation of sparsely populated on- and off-pathway folding intermediates, remain challenging to study experimentally.

Native-state hydrogen−deuterium exchange (HDX) experiments in concert with NMR[4,5] or mass spectrometric detection[6] have provided fundamental insights into the free energy surfaces of proteins that fold slowly with complex kinetics,[7] revealing the presence of subglobal cooperative folding units called "foldons".[8] The examination of kinetic folding pathways in a number of such proteins using HDX pulse labeling has shown a sequence of events that follows the order of stability of individual foldons.[9,10] This observation has led to the suggestion that protein folding proceeds via the ordered assembly of foldons, with the most stable foldons folding first.[8] Small single-domain proteins (less than approximately 100 residues), on the other hand, often fold without populating intermediates, indicating that their energy landscapes have simpler topographies.[11] It has been traditionally assumed that small single-domain proteins fold in a cooperative two-state fashion[12] as a result of a high free energy barrier separating their native and unfolded states. However, ultrafast kinetic methods have led to the discovery of many single-domain proteins that fold in only microseconds.[13] Such fast-folding proteins approach the folding speed limit, which has been estimated to be around 1 μs by many procedures, including estimates from the kinetics of secondary structure formation,[14] from the emergence of a second diffusive kinetic phase in some fast-folding proteins,[15] from the scaling of folding rates with protein size,[16] and more recently from the experimental study of folding transition path times.[17] For some fast-folding proteins, the free energy barrier is so low that the conformers at the barrier

Received: March 17, 2014
Published: April 28, 2014

   dx.doi.org/10.1021/ja502705y | J. Am. Chem. Soc. 2014, 136, 7444−7451

top are populated,[13] and thus, their equilibrium unfolding appears to be complex and probe-dependent, even though the underlying free energy landscape is essentially smooth.[18] Additionally, the recent implementation of submillisecond molecular dynamics simulations has indicated that such small fast-folding proteins also assemble their native structures in a stepwise manner.[19]

Fast-folding proteins are thus attractive targets for atomic-resolution experimental methods.[13] In this regard, relaxation dispersion (RD) NMR spectroscopy has evolved into an important technique for the structural characterization of local minima in the protein free energy landscape.[20−22] While such rare states do not give rise to detectable cross-peaks in NMR spectra, their presence causes broadening of resonances derived from the native state. In cases where the rates of interconversion between observable ("ground") and invisible ("conformationally excited") states are on the millisecond time scale, the magnitude of the exchange broadening can be systematically altered via a Carr−Purcell−Meiboom−Gill (CPMG) pulse train consisting of chemical shift refocusing pulses applied at varying frequencies (ν_{CPMG}). The graph of the effective transverse relaxation rate ($R_{2,eff}$) of a particular nucleus as a function of ν_{CPMG}, called the relaxation dispersion profile, can be fit to a model of conformational exchange to extract chemical shift differences for the nucleus in the native and invisible states. The chemical shifts so obtained have been used to solve the three-dimensional atomic-resolution structures of invisible states of proteins by incorporating them into chemical-shift-based structure prediction algorithms.[23,24] The structures of on-pathway folding intermediates of the FF module[25,26] and the Fyn SH3 domain[27] as well as a sparsely populated conformer of T4 lysozyme[28] and an Abp1p SH3/Ark peptide complex[29] have been obtained in this manner.

Here we employ RD NMR methodology to explore the energy landscape of the 62-residue protein gpW[30] from λ bacteriophage, which adopts an $\alpha + \beta$ fold in the native state with N- and C-terminal α-helices and an orthogonal β-hairpin (Figure 1A).[31] gpW is an ultrafast-folding protein with a folding time constant of ~8 μs at its melting temperature ($T_m \sim 67$ °C at pH 6.0).[30] RD NMR experiments reveal a sparsely and transiently populated invisible state (called X in what follows) in conformational exchange with native gpW. Chemical shifts of X obtained from the analysis of the RD NMR data show that the β-hairpin is locally unfolded in X whereas the two α-helices are intact, clearly establishing a hierarchy in the stability of structural units in this small protein. The detection and characterization of a low-lying thermally accessible partially unfolded state in gpW provides experimental evidence for the existence of a complex free energy landscape even for small proteins that fold very rapidly.

RESULTS

Relaxation Dispersion Measurements on gpW. The gpW protein folds in an ultrafast manner with a time constant of 8 μs at 67 °C and pH 6.0. In order to make the folding time scale accessible to RD NMR, which is limited to systems with exchange rates (k_{ex}) in the 100 $s^{-1} \leq k_{ex} \leq$ 2000 s^{-1} range (see below), we lowered the temperature to 1 °C, exploiting the steep temperature dependence of folding rates that is often observed for fast-folding proteins,[32] including gpW. The pH was also reduced to 3.5 in order to destabilize the protein in the hope that this would lead to increased populations of additional states along the landscape that would become amenable to study via the RD NMR approach. Notably, the structure of the native state of gpW remains unaffected by the low temperature and pH used in the present study. For example, the structures of gpW at 21 °C/pH 6.5[31] and 20 °C/pH 3.5 (Figure 1A) are virtually identical (a superposition is shown in Figure S1 in the Supporting Information). Furthermore, the patterns of amide ^{1}H and ^{15}N chemical shifts observed in the ^{1}H−^{15}N heteronuclear single-quantum correlation (HSQC) spectrum at 1 °C (Figure 1B) are very similar to those obtained at 25 °C, confirming that the available native-state structures are good models for gpW at 1 °C/pH 3.5. However, at the low temperature, the resonances show considerable differential line broadening (Figure 1B), and three of the 61 expected cross-peaks in the ^{1}H−^{15}N HSQC spectrum are broadened beyond detection, signifying the presence of micro- to millisecond conformational exchange.

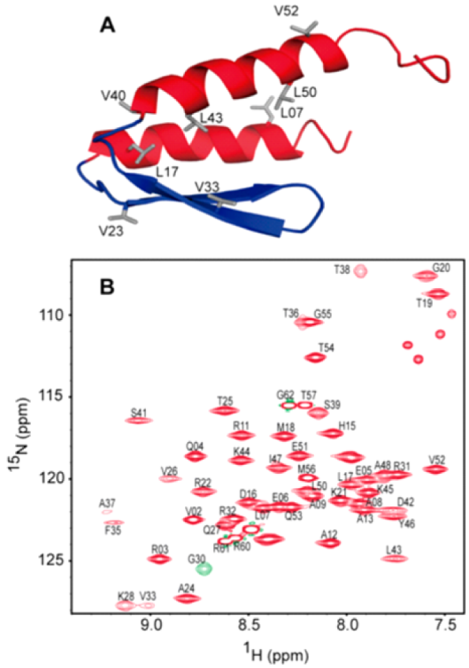

Figure 1. (A) Ribbon diagram of the structure of gpW, as determined by solution NMR analysis, at 20 °C and pH 3.5 (PDB ID 2L6R). The α-helical regions and terminal loops are colored red, the β-hairpin is shown in blue, and selected Val and Leu side chains have been highlighted in gray. (B) $^1H^N$−^{15}N HSQC spectrum of gpW at 1 °C and 11.7 T with assignments of resonances as indicated. The cross-peak shown in green is aliased.

In order to study the conformational exchange process in detail, a series of RD NMR experiments were performed. These provide structural information about thermally accessible conformational states that are not directly observable in NMR spectra so long as they are in equilibrium with the native state. The RD NMR measurements were carried out using backbone ^{15}N, $^1H^N$, $^{13}C^O$, and $^{13}C^\alpha$ probes to investigate the changes in secondary structure that accompany the exchange event and side-chain methyl-^{13}C nuclei to probe differences in hydrophobic packing of the native-state and invisible conformers. Well-resolved resonances belonging to 22 residues for ^{15}N, 32 for $^1H^N$, 24 for $^{13}C^\alpha$, and 25 for $^{13}C^O$ showed exchange contributions $R_{ex} >$ 5 s^{-1}, where $R_{ex} = R_{2,eff}(\nu_{CPMG} = \nu_{min}) - R_{2,eff}(\nu_{CPMG} = \infty)$, in which ν_{min} is the minimum CPMG pulsing frequency for a particular experiment (see the Experimental Section). Nonzero values of R_{ex} confirm the presence of one or more excited states in exchange with the native state. Representative RD profiles for a

dx.doi.org/10.1021/ja502705y | J. Am. Chem. Soc. 2014, 136, 7444−7451

number of spin probes in the α-helices (red and orange) and β-hairpin (blue and cyan) are shown in Figure 2.

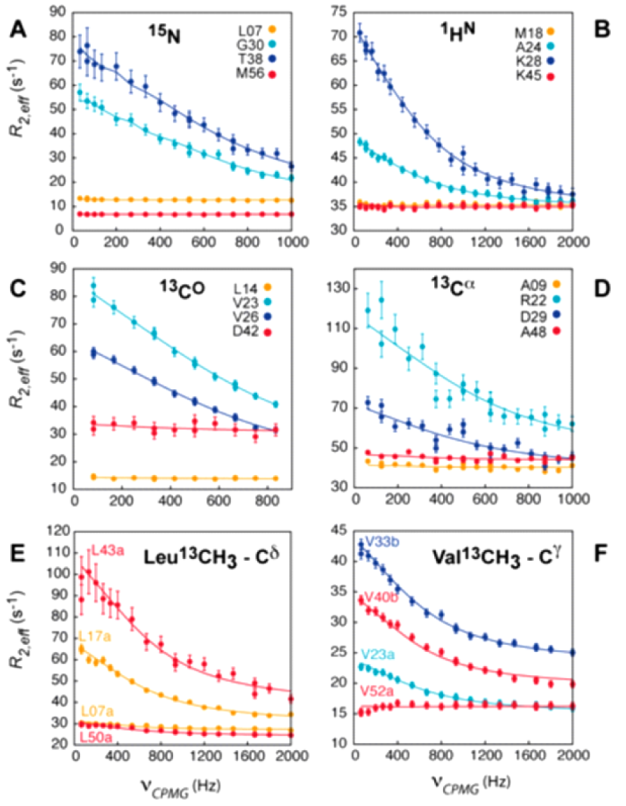

Figure 2. Relaxation dispersion profiles measured using A) ^{15}N, B) ^{1}H^{N}, C) ^{13}C^{O} and D) ^{13}C$^{\alpha}$ probes, recorded at 1 °C, 11.7 T, showing the existence of submillisecond time scale conformational fluctuations in gpW. Solid lines are best-fits of the data (circles) to a two-state exchange model. Vertical lines associated with each data point denote experimental errors. In general, dispersions (R_{ex} values) are larger for the residues located in the hairpin (cyan and blue) than for the residues in the helices (orange and red). E, F) Methyl-^{13}C dispersion profiles from Leu and Val residues. Stereospecific assignments of the prochiral methyl groups have not been obtained; pairs of methyl groups from a given side-chain are distinguished "a' and 'b", with 'a' corresponding to the methyl with the most upfield shifted resonance in the ^{13}C dimension.

Interestingly, the backbone nuclei of residues in the β-sheet show substantial exchange broadening, while the dispersion profiles of residues in the terminal α-helices are relatively flat, consistent with a smaller contribution from exchange. Thus, the exchange process is predominantly associated with the hairpin region of the structure. The CH_3-containing side chains that are localized within helices (e.g., residues L17 and L43; Figure 2E) and that form a part of the hydrophobic core are broadened considerably because of exchange. Thus, the hydrophobic packing may be altered in the invisible state, potentially as a result of a shift in the register of the helices. The CH_3 group of V33, which lies at the interface of the β-hairpin and α-helices, also has a large R_{ex} value (Figure 2F), either directly because of secondary structural changes in the β-hairpin or as a result of the relative motion between the helices and the hairpin. In addition, one of the methyl groups of residue V40, localized to the C-terminal helix at the beginning of the C-terminal helix, adjacent to the β-sheet, also has significant R_{ex} contributions (Figure 2F).

Obtaining Unique Populations and Extracting Structural Information. Relaxation dispersion profiles of ^{15}N, ^{1}H^{N}, and methyl-^{13}C spins with $R_{ex} > 5$ s^{-1} at both 11.7 and 18.8 T were fit globally to the Bloch−McConnell equations[33] appropriate for a model of two-site exchange,

$$X \underset{k_{NX}}{\overset{k_{XN}}{\rightleftarrows}} N$$

to extract $k_{ex} = k_{XN} + k_{NX} = 4087 \pm 42$ s^{-1}. The presence of a pronounced minimum in the graph of reduced χ^2 (χ^2_{red}) as a function of k_{ex} (Figure 3A) confirms the robustness of the fitted

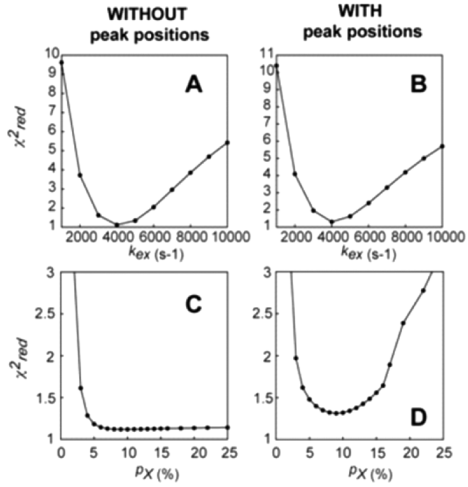

Figure 3. Variation of χ^2_{red} from fits of ^{15}N, ^{1}H^{N}, and methyl-^{13}C dispersion data at 1 °C as a function of the exchange parameters (A, B) k_{ex} and (C, D) p_X. Only RD CPMG data acquired at 11.7 and 18.8 T has been included in generating the data in (A) and (C), while the static magnetic field dependence of the native-state peak positions (based on HSQC and HMQC spectra acquired at 11.7 and 18.8 T) has also been included in the analysis in (B) and (D). It is clear that while a unique k_{ex} value, corresponding to a pronounced minimum in the χ^2_{red} vs k_{ex} profile in (A), can be obtained from fits of RD NMR data exclusively, a unique p_X can be obtained only when the RD NMR data are supplemented with the peak positions of the native state in HSQC/HMQC spectra recorded at a pair of static magnetic fields.

value of the exchange rate. This value of k_{ex} places the exchange process in the moderately fast regime, where for all but one or two spins in gpW it is the case that $k_{ex} > \Delta\omega$, where $\Delta\omega$ is the chemical shift difference (in rad/s) between the exchanging sites. For example, α values,[34] defining the chemical exchange time scale, range between 1.8 and 1.9 (with standard deviations of $\pm$0.3) for the different nuclei probed, where $\alpha = 2$ indicates fast exchange. The moderately fast exchange process challenges the extraction of a robust fractional population of the X state (p_X) because in this case only the product $p_X(1 - p_X)\Delta\omega^2$ can be obtained reliably from fits of RD data. The problem is illustrated in Figure 3C, where χ^2_{red} from fits of dispersion profiles is plotted as a function of p_X. The flat χ^2_{red} versus p_X curve indicates that the dispersion profiles can be fit equally well to virtually any value of $p_X > 5\%$, with a concomitant adjustment of $\Delta\varpi$ (in ppm) to maintain the quality of the fit. Since structural information on X is obtained from chemical shift differences, a reliable estimate of p_X becomes imperative.

It has recently been shown that the correlation between p_X and $\Delta\omega$ can be broken for k_{ex} values as large as 4000−6000 s^{-1} by exploiting the fact that the peak line widths and positions depend in different ways on $k_{ex}/\Delta\omega$ and hence on the static magnetic field.[35] Thus, simultaneously fitting the relaxation dispersion

dx.doi.org/10.1021/ja502705y | J. Am. Chem. Soc. 2014, 136, 7444−7451

profiles and the positions of correlations in spectra recorded at a number of static magnetic fields can extend the exchange time scale of systems that are amenable to study by RD NMR. Here we recorded $^{1}H-^{15}N$ HSQC and heteronuclear multiple-quantum correlation (HMQC) spectra at 11.7 and 18.8 T and measured the shifts in peak positions in the HSQC and HMQC data sets and between the HSQC data sets. Including these shifts along with ^{15}N, $^{1}H^{N}$, and methyl-^{13}C dispersion profiles in the fits breaks the correlation between p_X and $\Delta\varpi$, producing a distinct minimum in the χ^2_{red} versus p_X plot at $p_X = 9.0 \pm 0.3\%$ (Figure 3D). It is worth noting that in the (moderately) fast exchange limit that is germane here, $\Delta\varpi$ scales as $p_X^{0.5}$. Thus, errors in p_X on the order of 30−40% lead to changes in chemical shift values of no more than 15−20%, which have a negligible effect on the structural insights that can be obtained (see below).

Structural Features of the Sparsely Populated State. Once accurate exchange parameters were determined, ^{15}N, $^{1}H^{N}$, $^{13}C^{O}$, $^{13}C^{\alpha}$, and methyl-^{13}C chemical shifts of the invisible state were obtained by fitting the RD profiles to a simple model of two-state exchange with k_{ex} and p_X fixed. Large ^{15}N chemical shifts (>4 ppm) were observed for some backbone ^{15}N nuclei, suggesting that the protein may undergo partial unfolding. To ascertain whether this is the case, differences between ^{15}N chemical shifts in the native and invisible states ($\Delta\varpi_{exp} = \Delta\varpi_{XN} = \varpi_X - \varpi_N$) were plotted against the corresponding values that would be expected for a global folding−unfolding transition ($\Delta\varpi_{pred} = \Delta\varpi_{UN}$) (Figure 4A). Intriguingly, the pattern obtained shows a distinct bimodal distribution, with chemical shift differences for residues in the β-sheet correlating very well with the $\Delta\varpi_{UN}$ values while the analogous values for the α-helices show a much poorer correlation. Other backbone nuclei (Figure 4B−D), in particular $^{13}C^{\alpha}$ and $^{13}C^{O}$, which are sensitive to secondary structure changes,[36] mirror the bimodal distribution pattern observed for ^{15}N, confirming that the β-sheet is indeed unfolded in the invisible state. The $^{13}C^{\alpha}$ and $^{13}C^{O}$ chemical shift data are further consistent with the helices remaining intact in X, as established by the secondary structure program TALOS+.[37] Because the signs of the $\Delta\varpi_{XN}$ values were not available for many of the ^{13}C probes, we assumed the most extreme scenario in our analysis of the helical residues, where in the absence of the sign ϖ_X was arbitrarily chosen to be closer to the value expected for a random-coil conformer (Figure S2 in the Supporting Information). Even with this extreme assumption, the helices are preserved in the excited state of gpW. The graph of the residue-specific variation in backbone chemical shifts, $\Delta\varpi_{RMS}$ (Figure 5), shows that significant chemical shift changes are localized to the central β-sheet region ($\langle\Delta\varpi_{RMS}\rangle = 0.7 \pm 0.3$) with much smaller shifts for the flanking helices ($\langle\Delta\varpi_{RMS}\rangle = 0.2 \pm 0.1$ and 0.2 ± 0.2 for helices 1 and 2, respectively). To summarize, the chemical shift data establish that in X the β-hairpin is unfolded but the α-helices remain intact.

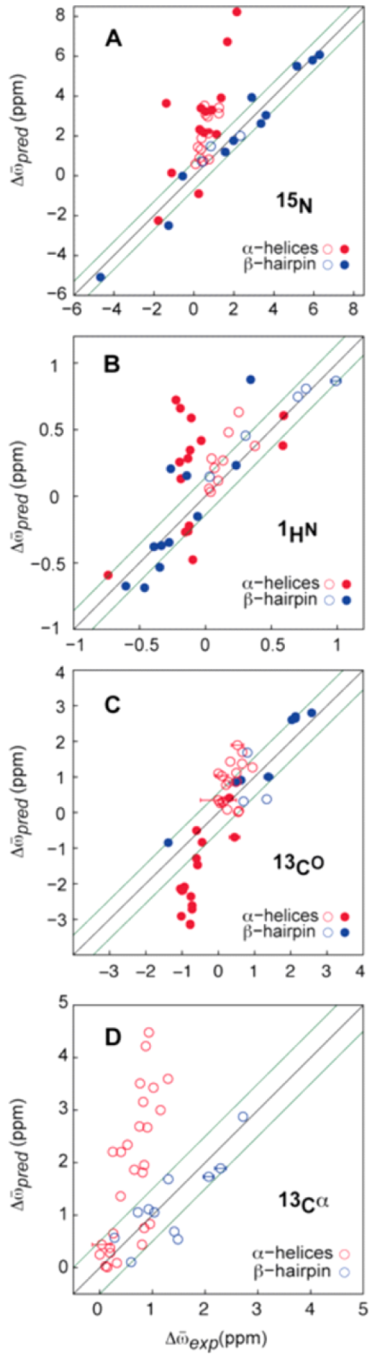

Figure 4. Comparison of experimentally obtained chemical shift differences between the native and X states of gpW at 1 °C ($\Delta\varpi_{exp} = \varpi_X - \varpi_N$) for (A) ^{15}N, (B) $^{1}H^{N}$, (C) $^{13}C^{O}$, and (D) $^{13}C^{\alpha}$ spins with the corresponding values expected if X were in a random-coil conformation ($\Delta\varpi_{pred} = \varpi_U - \varpi_N$). The red (blue) circles denote values derived for residues belonging to helical (hairpin) regions. Values for which the signs of $\Delta\varpi$ have (have not) been obtained experimentally are denoted by solid (open) circles; for the cases where signs are not available, values of $|\Delta\varpi_{exp}|$ and $|\Delta\varpi_{pred}|$ are plotted. Error bars smaller than the circle diameter have not been explicitly shown. The black line is $y = x$, and the region between the green lines corresponds to the uncertainty in $\Delta\varpi_{pred}$ based on the error in predicted ϖ_U values (from ref 64).

DISCUSSION

The RD NMR approach is particularly powerful for characterizing low-populated protein conformational substates because of the large number of probes that can be used, allowing detailed atomic-resolution structural information to be obtained.[38] This approach has led to the determination of the structures of on-pathway folding intermediates in the native protein free energy landscapes for the slower-folding FF[25,26] and Fyn SH3[27] domains (millisecond time scale). The FF domain folding intermediate is particularly interesting in that helix 3 is significantly longer than in the native state, leading to the establishment of non-native interactions across the protein.[25,26] These alternative conformations produce local minima in the free energy surface from which the protein must escape before reaching the native structure.

dx.doi.org/10.1021/ja502705y | J. Am. Chem. Soc. 2014, 136, 7444−7451

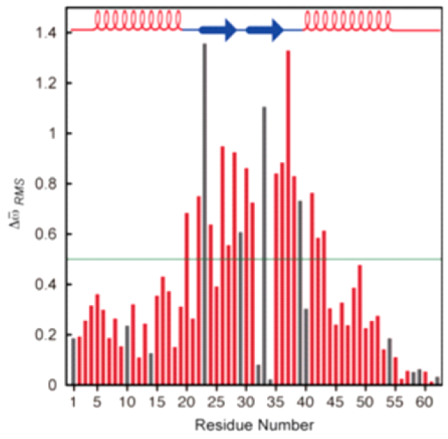

Figure 5. Values of $\Delta\varpi_{RMS}$ plotted vs residue number. $\Delta\varpi_{RMS} = [(1/N)\sum_i(\Delta\varpi_i/\Delta\varpi_{i,STD})^2]^{1/2}$, where $\Delta\varpi_i$ is the difference between the shifts in the native and X states for a particular nucleus in a given residue, $\Delta\varpi_{i,STD}$ corresponds to one standard deviation of the distribution of chemical shifts for that nucleus in the context of the amino acid in question, obtained from a database of protein chemical shifts [Biological Magnetic Resonance Data Bank (BMRB); http://www.bmrb.wisc.edu/], and N is the number of nuclei included in the summation ($\leq$4). The nuclei considered are ^{15}N, ^{1}H^{N}, ^{13}C$^{\alpha}$, and ^{13}C^{O}. Bars representing values obtained when only two or fewer $\Delta\varpi$ values were included are colored in gray. Some of these residues (A10, L14, E34, E49, Q58, R59) were overlapped in the ^{1}H^{N}–^{15}N HSQC data sets, while others (V23, D29, V33, V40) were too broad because of exchange, making it impossible to obtain reliable shift differences.

Proteins that fold in a two-state manner have been a major focus of interest in folding studies via mutational analysis.[39] In principle, these proteins have free energy landscapes devoid of local minima that could be probed by RD NMR. Work over the last 15 years on fast folding, however, has described a new class of proteins that approach the folding speed limit[40] and thus have free energy surfaces with very low barriers and shallow minima.[13] The shallowness of ultrafast-folding free energy surfaces allows ensembles of partially folded conformations, which would correspond to excited states in nominally two-state folding, to become populated under certain experimental conditions.[13] These low-populated partially folded conformations can be detected by differential scanning calorimetry,[41] giving the appearance of complex unfolding behavior in equilibrium[18] and kinetics[42] experiments, even though the underlying energy landscapes are smooth. The special characteristics of fast-folding proteins have been dramatically demonstrated in recent long-time-scale atomistic simulations that achieved multiple folding and unfolding events for 12 such proteins.[19] The simulations identified a general theme whereby assembly of the native structures for these proteins occurs in a stepwise fashion with the formation of key secondary structural elements at an early stage of folding that then template the formation of the rest of the secondary structure as well as the establishment of long-range native contacts. Fast-folding proteins thus seem to accrue structure in steps rather than in a globally cooperative way.

Experimentally, the coarse features of fast-folding free energy surfaces have been derived from fits of data from multiple probes to statistical-mechanical models.[30,42] An ultrafast-folding protein in which the topography of the free energy surface has been characterized in detail is the villin subdomain.[43] In other cases, such as the engrailed homeodomain (EnHD)[44] and Trp cage,[45] similar experimental observations have been interpreted as evidence for the formation of an on-pathway intermediate. However, only in a very few examples have these partially folded conformational ensembles been characterized in structural detail via experiment. One example is the three-helix-bundle EnHD intermediate, where a mutant was studied that adopts the partly folded conformation at low ionic strength and folds to the native state under conditions of high ionic strength.[46] Motivated by our prior work on the slower-folding FF and Fyn SH3 domains and by the fact that rich conformational behavior has been observed for fast-folding proteins by a variety of biophysical techniques,[13] we wished to extend our RD NMR studies to the exploration of the free energy landscapes of more rapidly folding molecules. Studies of fast-folding proteins by RD NMR are technically challenging, however, and this was the case for the gpW protein studied here. Folding of gpW has been investigated previously using a variety of different spectroscopic techniques, and a folding relaxation rate of 125 000 s^{-1} has been measured at 67 °C.[30] Conformational exchange events on this time scale are well outside the window of RD NMR, which in general is sensitive to processes that are more than an order of magnitude slower. However, exchange rates can be manipulated by changing the temperature, and for gpW at 1 °C and pH 3.5, the exchange was sufficiently slowed to allow RD profiles with significant R_{ex} values to be recorded for ^{15}N, ^{1}H^{N}, ^{13}C^{O}, ^{13}C$^{\alpha}$, and methyl-^{13}C nuclei, as illustrated in Figure 2. These were fit well to a two-site exchange process with a rate of interconversion of 4100 s^{-1} ($\chi^2_{red} \sim 1$; Figure 3), which remains relatively fast on the chemical shift time scale. In this exchange regime it is not possible to obtain accurate chemical shift differences between exchanging sites from analysis of dispersion profiles because of the coupling between the values of p_X and $\Delta\omega$. This coupling can be broken, however, through simultaneous fits of both RD data and the chemical shifts of ground-state resonances as functions of the static magnetic field, as illustrated in Figure 3. A p_X value of 9% was obtained through a combined analysis of this sort, along with chemical shifts that could be used to obtain structural information about state X. Notably, the excited state retains the terminal α-helices of the native conformation of gpW while the β-hairpin that connects the helices is unfolded (Figures 4 and 5). There is thus a hierarchical ordering of structural stability even in this small protein, with the β-hairpin emerging as a subglobal autonomously folding structural unit, or "foldon".

The partially unfolded state characterized in this study is likely a folding intermediate, though there is no direct kinetic evidence from our NMR experiments because they were recorded under conditions where the population of the fully unfolded state is negligible. Instead, we remeasured the overall folding–unfolding relaxation kinetics of gpW by temperature-jump IR spectroscopy, but this time at pH 3.5 (Figure 6A). We could not reach 1 °C directly with T-jump experiments because of the lack of kinetic amplitude under conditions that are so far from the folding midpoint. However, quantitative analysis of the temperature-dependent rate with a simple free energy surface (FES) model (see the Supporting Information) produced an extrapolated rate constant of 5000 ± 100 s^{-1} at 1 °C, where the uncertainty in the extrapolated rate was estimated using a jackknife analysis[47] (±100 s^{-1} is one standard deviation in the rates obtained from the analysis). The obtained value is in reasonable agreement with the value of k_{ex} that we measured by RD NMR at this temperature (4087 ± 42 s^{-1}), especially considering that the extrapolation is over 20 °C and that $\Delta C_{p,res}$ in the FES model is fixed (see the Supporting Information). The similarity in rates suggests that the formation of the X state described here corresponds to the rate-limiting step in gpW unfolding. On the

dx.doi.org/10.1021/ja502705y | J. Am. Chem. Soc. 2014, 136, 7444–7451

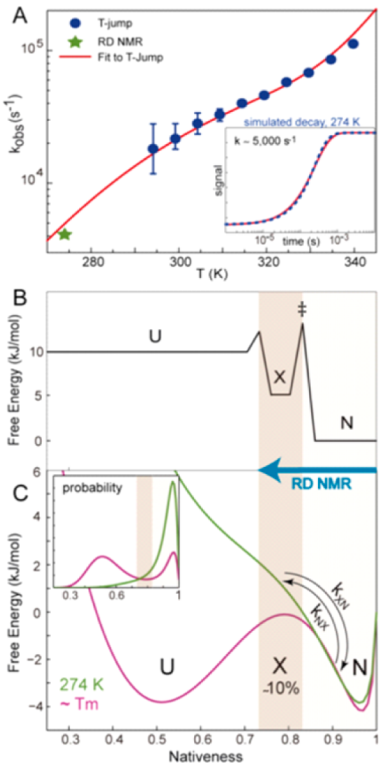

Figure 6. Mechanistic interpretation of the invisible state *X* in light of the comparison between the RD NMR results and the results of laser-induced temperature-jump experiments. (A) Folding−unfolding relaxation kinetics measured by infrared *T*-jump at pH 3.5 (blue circles) fitted to a 1D FES model (red curve; see the Supporting Information), k_{ex} from RD NMR (green star), and the relaxation decay at 1 °C as simulated by the FES model (blue in inset) together with a single-exponential fit for reference (red in inset). (B) Schematic representation of the FES in terms of a chemical kinetics model that separates the *U*, *X*, and *N* states with barriers. (C) The FESs (main) and probability distributions (inset) obtained for gpW at the denaturation midpoint (magenta) and at 1 °C (green), including the region populated by the invisible state *X*. It is noteworthy that the NMR data cannot distinguish between the models in (B) and (C).

basis of a chemical kinetics interpretation, which is most commonly used for RD NMR data, *X* would thus be an on-pathway intermediate placed between the unfolded state and the global transition state, corresponding to a local minimum in the free energy surface (Figure 6B). The FES analysis of the *T*-jump data offers an alternative interpretation in which *X* corresponds to the ensemble of partly folded conformations placed at the top of the low-barrier transition observed by IR spectroscopy near T_m (Figure 6C). Under highly stabilizing conditions such as a temperature of 1 °C, the FES of gpW is predicted to become downhill (green surface in Figure 6C), but the ensemble ascribed to *X* remains the first excited state that is sampled from *N*, interconverting with nearly single-exponential kinetics (Figure 6A inset) and making up ∼10% of the total population (Figure 6C inset), consistent with the RD NMR results. Unlike the model of Figure 6B, *X* does not occupy a local minimum but rather is localized at the saddle point in the FES. In addition, the kinetics are governed essentially by the friction along the landscape, which in turn is reflected by the temperature dependence of the diffusion on the surface (determined by the intramolecular diffusion coefficient; see eq S5 in the Supporting Information). The RD NMR data do not distinguish between these two possible models and, as described above, are consistent with a two-state interconversion between the *N* and *X* states.

Regardless of the preferred interpretation, *X* emerges in both cases as a productive intermediate occurring late in the kinetic folding pathway of gpW to its native conformation. Because in *X* the α-helices are fully formed while the β-hairpin is unfolded, the formation of the β-hairpin may represent the very last step in gpW folding. Interestingly, this conclusion is consistent with the empirical observation that spectroscopic probes sensitive to tertiary interactions between the β-hairpin and the α-helices report a lower stability than probes sensitive to the α-helix structure alone.[30] Moreover, the lower intrinsic stability of the hairpin has also been observed in long-time-scale molecular dynamics simulations of gpW. Finally, we performed ^{15}N RD measurements on a sample of gpW at 1 °C and pH 6.5 to establish whether the intermediate that we have characterized in this work is likely to be important at neutral pH. Notably, the extracted $|\Delta\varpi_{XN}|$ values are in good agreement with those obtained at pH 3.5 (Figure S3 in the Supporting Information), providing strong evidence that the excited state remains intact over a broad range of pH values.

CONCLUSIONS

In summary, using a combined analysis of RD profiles and the dependence of native-state peak positions on the static magnetic field, we have been able to probe the free energy landscape of the fast-folding α/β gpW domain using solution NMR spectroscopy. We have identified and structurally characterized a thermally accessible sparsely formed, transiently populated state in equilibrium with the native state of gpW. The structure of this "invisible" state clearly establishes the presence of a hierarchy in the stability of secondary structural elements and the existence of a complex folding process even for this small (62-residue) fast-folding protein. gpW is considered to be an incipient downhill-folding protein with a small (∼*RT*) free energy barrier at its T_m (∼67 °C at pH 6.0).[30] A previous study suggested that a combination of strong local interactions and loose hydrophobic packing might contribute to a lowering of the folding free energy barrier.[30] Our NMR characterization of the invisible state now confirms the involvement of both of these factors in shaping the free energy surface of gpW. Strong local interactions ensure that the N- and C-terminal helices remain structured in the *X* state characterized here, while RD data for Leu and Val residues involved in tertiary interactions strongly suggest that the hydrophobic core is disrupted in the invisible state. The ability to extend RD NMR to faster exchange processes, as described here, increases the range of protein systems that can be studied via this methodology and opens up the exciting possibility of characterizing in greater detail than heretofore possible the free energy landscapes that dictate protein function.

EXPERIMENTAL SECTION

Protein Expression and Purification. A 62-residue gpW construct that did not include the C-terminal six residues that induce aggregation[30] was chosen for the current study. The T2V mutation present in the construct used in previous structural studies of this protein[30,31] was retained. *Escherichia coli* BL21(DE3) cells expressing gpW with a C-terminal histidine tag were grown at 37 °C in minimal medium. Protein expression was induced with isopropyl-β-D-thiogalactopyranoside (IPTG) when the cell culture reached an optical density at 600 nm (OD_{600}) value of 0.7−0.8. After 4 h of growth at 37 °C, the cells were harvested and centrifuged at 8000 rpm for 30 min. The pellet was resuspended in buffer (20 mM Tris, 150 mM NaCl, 8 M urea, pH 8) until homogeneous. The lysate was ultracentrifuged at 18 000 rpm for

dx.doi.org/10.1021/ja502705y | J. Am. Chem. Soc. 2014, 136, 7444−7451

45 min, and the supernatant was gently sonicated, loaded onto a Ni affinity column, and eluted with an imidazole gradient. After fractions containing gpW were pooled, the imidazole was subsequently dialyzed out, and the His tag was cleaved by incubation with Ulp1 protease for 1 h at 37 °C. A second run through the Ni column was used to remove the cleaved His tag. The protein was then concentrated with a 3 kDa molecular weight cutoff Centricon centrifugal concentrator for a last reversed-phase (RP) HPLC step using a 0−95% water/acetonitrile gradient with 0.1% trifluoroacetic acid to remove salts and other impurities. Fractions containing pure gpW were pooled and lyophilized. The purity of the protein was checked by sodium dodecyl sulfate polyacrylamide gel electrophoresis, and its identity verified by electrospray ionization mass spectrometry.

Sample Preparation for NMR Spectroscopy. Uniformly ^{15}N-labeled and selectively methyl-^{13}C-labeled gpW, expressed in minimal medium containing $^{15}NH_4Cl$ and [1-^{13}C]glucose as the sole nitrogen and carbon sources, respectively,[48] was used to perform ^{15}N, $^{1}H^{N}$, and $^{13}CH_3$ RD experiments. [U-^{15}N,^{13}C]gpW was expressed in minimal medium containing $^{15}NH_4Cl$ and [$^{13}C_6$]glucose, while uniformly ^{15}N-labeled and selectively C^{α}-labeled gpW was produced using minimal medium with $^{15}NH_4Cl$ and [2-^{13}C]glucose.[48] These samples were used for $^{13}C^{O}$ and $^{13}C^{\alpha}$ dispersion measurements, respectively. All of the NMR samples comprised approximately 1 mM protein in 20 mM glycine buffer (pH 3.5), 1 mM sodium azide, 10% D_2O/90% H_2O.

NMR Spectroscopy and Data Analysis. Backbone and side-chain chemical shift assignments were obtained using standard triple-resonance experiments[49] performed at either 11.7 or 14.1 T and 1 °C. RD data were recorded at field strengths of 11.7 and 18.8 T at 1 °C, with the temperature measured using a thermocouple inserted into an NMR tube. ^{15}N, $^{1}H^{N}$, $^{13}C^{O}$, $^{13}C^{\alpha}$, and methyl-^{13}C RD profiles were recorded with pulse schemes described previously.[50−55] For the measurement of $^{1}H^{N}$ dispersions, a modified sequence was used wherein the amide magnetization at the start of the constant-time CPMG element was antiphase with respect to ^{15}N. In addition, a (backbone-amide-specific) REBURP pulse of 2.00 ms (11.7 T) or 1.25 ms (18.8 T) duration was applied on the ^{15}N channel during the first INEPT transfer period in experiments recording ^{15}N and $^{1}H^{N}$ profiles to eliminate intense side-chain correlations arising from Arg residues. A prescan delay of 2.5 s was used in all cases, with constant-time CPMG relaxation delays of 30, 18, 24, 16, and 30 ms for measurements of ^{15}N, $^{1}H^{N}$, $^{13}C^{O}$, $^{13}C^{\alpha}$, and methyl-^{13}C RD profiles, respectively. Dispersion data were collected at 17 CPMG fields ranging from 33.3 to 1000 Hz for ^{15}N (11.7 and 18.8 T), 21 CPMG fields ranging from 55.6 to 2000 Hz for $^{1}H^{N}$ (11.7 and 18.8 T), 10 (12) CPMG fields from 83.3 to 833.3 (1000) Hz for $^{13}C^{O}$ at 11.7 T (18.8 T), 10 (13) CPMG fields from 62.5 to 1000 Hz for $^{13}C^{\alpha}$ at 11.7 T (18.8 T), and 17 CPMG fields ranging from 66.7 to 2000 Hz for $^{13}CH_3$ (11.7 and 18.8 T). Errors in $R_{2,\mathrm{eff}}$ were estimated by acquiring at least three duplicate points at selected ν_{CPMG} values.

Additional experiments were performed to determine the signs of the chemical shift differences, $\Delta\varpi$, obtained from fits of CPMG RD data. For ^{15}N $\Delta\varpi$ values, signs were obtained by comparing the peak positions in $^{1}H^{N}$−^{15}N HSQC spectra acquired at 11.7 and 18.8 T and in $^{1}H^{N}$−^{15}N HSQC and HMQC spectra,[56] also measured at 11.7 and at 18.8 T. The signs of $^{1}H^{N}$ shift differences were obtained from an analysis of $^{1}H^{N}/^{15}$N zero- and double-quantum coherence RD profiles[57] and also from a comparison of the direct-dimension chemical shifts in HSQC spectra recorded at 11.7 and 18.8 T.[58] Signs for $^{13}C^{O}$ $\Delta\varpi$ values were obtained from a comparison of resonance positions in $^{1}H^{N}$−$^{13}C^{O}$ data sets recorded at 11.7 and 18.8 T where the $^{13}C^{O}$ chemical shift derives from evolution of either single- or multiple-quantum ($^{1}H^{N}$−$^{13}C^{O}$ or ^{15}N−$^{13}C^{O}$) coherence.[59] In total, 31, 26, and 25 signs were determined for 53, 52, and 47 measured ^{15}N, $^{1}H^{N}$, and $^{13}C^{O}$ $\Delta\varpi$ values. It was not possible to measure signs for $^{13}C^{\alpha}$ shift differences because of the limited quality of $^{1}H^{\alpha}$−$^{13}C^{\alpha}$ correlation maps.

NMR data were analyzed using the NMRPipe suite of programs,[60] with peak intensities quantified using FuDA (http://pound.med.utoronto.ca/software.html) as previously described.[61] Spectra were visualized with NMRDraw[60] and Sparky.[62] Exchange parameters (p_X, k_{ex}, $\Delta\varpi$) were obtained by simultaneously fitting the dispersion profiles and HSQC/HMQC data to a global two-site exchange model using the program CHEMEX (written in-house, available upon request) that numerically propagates the Bloch−McConnell equations[33] in the simulation of the experimental data.

Infrared Temperature-Jump Kinetics. gpW samples for infrared kinetic measurements were prepared at a protein concentration of 4 mg/mL in 20 mM deuterated glycine buffer after achieving complete deuteration of the exchangeable amide protons by performing multiple cycles of lyophilization and dilution in D_2O. The samples were adjusted to pD 3.5 after correction for the isotope artifact on the readout of the glass electrode of the pH meter. Infrared laser-induced *T*-jump measurements were performed using a custom-built apparatus.[63] Briefly, the fundamental wavelength of a Nd:YAG laser (Continuum Surelite I) operating at a repetition rate of 4 Hz is shifted to 1907 nm (a frequency at which D_2O exhibits strong absorption) by passing the laser pulses through a 1 m path Raman cell (Light Age Inc.) filled with a high-pressure mixture of H_2 and Ar. The output of the Raman cell is <10 ns pulses with an energy of about 30 mJ/pulse, which induce a local temperature jump of about 10−12 °C when focused onto the sample. The response of the sample to this fast perturbation is monitored using a quantum cascade laser tunable over the range 1605−1690 cm^{-1} (Daylight Solutions) to probe the amide I band of the protein under study. For gpW we tuned the laser to 1632 cm^{-1} to match the absorption maximum of the α-helix amide I band. The light transmitted from the sample is then detected using a fast mercury cadmium telluride (MCT) detector (Kolmar Technologies) coupled to an oscilloscope (Tektronix DPO4032). Samples were held in a cell formed by two MgF_2 windows separated by a 50 μm Teflon spacer and thermostated at the proper base temperature using two Peltier thermoelectric coolers (TE Technology Inc.) in a custom-built sample holder. The transmission of D_2O was used as an internal thermometer to measure the amplitude of the temperature jump.

■ ASSOCIATED CONTENT

Supporting Information

Description of the FES model; figures showing the superposition of the NMR-derived structures of gpW at pH 3.5 and 6.5, establishing that the α-helices are intact in the excited state of gpW, and providing evidence that state *X* characterized at pH 3.5 is populated at neutral pH as well; and tables of NMR chemical shifts. This material is available free of charge via the Internet at http://pubs.acs.org.

■ AUTHOR INFORMATION

Corresponding Authors

kay@pound.med.utoronto.ca
vmunoz@cnb.csic.es

Notes

The authors declare no competing financial interest.

■ ACKNOWLEDGMENTS

C.S.-M. acknowledges support from the Spanish Ministry of Economy and Competitiveness in the form of a predoctoral fellowship (BES-2009-029117). A.S. was the recipient of a postdoctoral fellowship from the Canadian Institutes of Health Research (CIHR). This work was funded through CIHR and NSERC research grants to L.E.K. and Grants CSD2009-00088 and BIO2011-28092 (Spanish Ministry of Economy and Competitiveness) and ERC-2012-ADG-323059 to V.M. L.E.K. holds a Canada Research Chair in Biochemistry.

■ REFERENCES

(1) Boehr, D. D.; Nussinov, R.; Wright, P. E. *Nat. Chem. Biol.* **2009**, *5*, 789−796.
(2) Frauenfelder, H.; Sligar, S. G.; Wolynes, P. G. *Science* **1991**, *254*, 1598−1603.

(3) Lazaridis, T.; Karplus, M. *Biophys. Chem.* **2003**, *100*, 367−395.
(4) Bai, Y.; Sosnick, T. R.; Mayne, L.; Englander, S. W. *Science* **1995**, *269*, 192−197.
(5) Chamberlain, A. K.; Handel, T. M.; Marqusee, S. *Nat. Struct. Mol. Biol.* **1996**, *3*, 782−787.
(6) Hu, W.; Walters, B. T.; Kan, Z.-Y.; Mayne, L.; Rosen, L. E.; Marqusee, S.; Englander, S. W. *Proc. Natl. Acad. Sci. U.S.A.* **2013**, *110*, 7684−7689.
(7) Bai, Y. *Chem. Rev.* **2006**, *106*, 1757−1768.
(8) Maity, H.; Maity, M.; Krishna, M. M.; Mayne, L.; Englander, S. W. *Proc. Natl. Acad. Sci. U.S.A.* **2005**, *102*, 4741−4746.
(9) Hoang, L.; Bédard, S.; Krishna, M. M.; Lin, Y.; Englander, S. W. *Proc. Natl. Acad. Sci. U.S.A.* **2002**, *99*, 12173−12178.
(10) Chamberlain, A. K.; Marqusee, S. *Adv. Protein Chem.* **2000**, *53*, 283−328.
(11) Bartlett, A. I.; Radford, S. E. *Nat. Struct. Mol. Biol.* **2009**, *16*, 582−588.
(12) Jackson, S. E. *Folding Des.* **1998**, *3*, R81−R91.
(13) Muñoz, V. *Annu. Rev. Biophys. Biomol. Struct.* **2007**, *36*, 395−412.
(14) Eaton, W. A.; Muñoz, V.; Thompson, P. A.; Henry, E. R.; Hofrichter, J. *Acc. Chem. Res.* **1998**, *31*, 745−753.
(15) Yang, W. Y.; Gruebele, M. *Nature* **2003**, *423*, 193−197.
(16) Naganathan, A. N.; Muñoz, V. *J. Am. Chem. Soc.* **2005**, *127*, 480−481.
(17) Chung, H. S.; McHale, K.; Louis, J. M.; Eaton, W. A. *Science* **2012**, *335*, 981−984.
(18) Garcia-Mira, M. M.; Sadqi, M.; Fischer, N.; Sanchez-Ruiz, J. M.; Muñoz, V. *Science* **2002**, *298*, 2191−2195.
(19) Lindorff-Larsen, K.; Piana, S.; Dror, R. O.; Shaw, D. E. *Science* **2011**, *334*, 517−520.
(20) Palmer, A. G.; Kroenke, C. D.; Loria, J. P. *Methods Enzymol.* **2001**, *339*, 204−238.
(21) Mittermaier, A.; Kay, L. E. *Science* **2006**, *312*, 224−228.
(22) Palmer, A. G., III; Massi, F. *Chem. Rev.* **2006**, *106*, 1700−1719.
(23) Robustelli, P.; Kohlhoff, K.; Cavalli, A.; Vendruscolo, M. *Structure* **2010**, *18*, 923−933.
(24) Shen, Y.; Lange, O.; Delaglio, F.; Rossi, P.; Aramini, J. M.; Liu, G.; Eletsky, A.; Wu, Y.; Singarapu, K. K.; Lemak, A. *Proc. Natl. Acad. Sci. U.S.A.* **2008**, *105*, 4685−4690.
(25) Korzhnev, D. M.; Religa, T. L.; Banachewicz, W.; Fersht, A. R.; Kay, L. E. *Science* **2010**, *329*, 1312−1316.
(26) Korzhnev, D. M.; Vernon, R. M.; Religa, T. L.; Hansen, A. L.; Baker, D.; Fersht, A. R.; Kay, L. E. *J. Am. Chem. Soc.* **2011**, *133*, 10974−10982.
(27) Neudecker, P.; Robustelli, P.; Cavalli, A.; Walsh, P.; Lundström, P.; Zarrine-Afsar, A.; Sharpe, S.; Vendruscolo, M.; Kay, L. E. *Science* **2012**, *336*, 362−366.
(28) Bouvignies, G.; Vallurupalli, P.; Hansen, D. F.; Correia, B. E.; Lange, O.; Bah, A.; Vernon, R. M.; Dahlquist, F. W.; Baker, D.; Kay, L. E. *Nature* **2011**, *477*, 111−114.
(29) Vallurupalli, P.; Hansen, D. F.; Kay, L. E. *Proc. Natl. Acad. Sci. U.S.A.* **2008**, *105*, 11766−11771.
(30) Fung, A.; Li, P.; Godoy-Ruiz, R.; Sanchez-Ruiz, J. M.; Muñoz, V. *J. Am. Chem. Soc.* **2008**, *130*, 7489−7495.
(31) Sborgi, L.; Verma, A.; Muñoz, V.; de Alba, E. *PLoS One* **2011**, *6*, No. e26409.
(32) Naganathan, A. N.; Doshi, U.; Muñoz, V. *J. Am. Chem. Soc.* **2007**, *129*, 5673−5682.
(33) McConnell, H. M. *J. Chem. Phys.* **1958**, *28*, 430−431.
(34) Millet, O.; Loria, J. P.; Kroenke, C. D.; Pons, M.; Palmer, A. G., III. *J. Am. Chem. Soc.* **2000**, *122*, 2867−2877.
(35) Vallurupalli, P.; Bouvignies, G.; Kay, L. E. *J. Phys. Chem. B* **2011**, *115*, 14891−14900.
(36) Wishart, D. S.; Bigam, C. G.; Holm, A.; Hodges, R. S.; Sykes, B. D. *J. Biomol. NMR* **1995**, *5*, 67−81.
(37) Shen, Y.; Delaglio, F.; Cornilescu, G.; Bax, A. *J. Biomol. NMR* **2009**, *44*, 213−223.
(38) Baldwin, A. J.; Kay, L. E. *Nat. Chem. Biol.* **2009**, *5*, 808−814.
(39) Naganathan, A. N.; Muñoz, V. *Proc. Natl. Acad. Sci. U.S.A.* **2010**, *107*, 8611−8616.
(40) Kubelka, J.; Hofrichter, J.; Eaton, W. A. *Curr. Opin. Struct. Biol.* **2004**, *14*, 76−88.
(41) Naganathan, A. N.; Sanchez-Ruiz, J. M.; Muñoz, V. *J. Am. Chem. Soc.* **2005**, *127*, 17970−17971.
(42) Li, P.; Oliva, F. Y.; Naganathan, A. N.; Muñoz, V. *Proc. Natl. Acad. Sci. U.S.A.* **2009**, *106*, 103−108.
(43) Kubelka, J.; Henry, E. R.; Cellmer, T.; Hofrichter, J.; Eaton, W. A. *Proc. Natl. Acad. Sci. U.S.A.* **2008**, *105*, 18655−18662.
(44) Religa, T. L.; Johnson, C. M.; Vu, D. M.; Brewer, S. H.; Dyer, R. B.; Fersht, A. R. *Proc. Natl. Acad. Sci. U.S.A.* **2007**, *104*, 9272−9277.
(45) Neuweiler, H.; Doose, S.; Sauer, M. *Proc. Natl. Acad. Sci. U.S.A.* **2005**, *102*, 16650−16655.
(46) Religa, T.; Markson, J.; Mayor, U.; Freund, S.; Fersht, A. *Nature* **2005**, *437*, 1053−1056.
(47) Press, W. H.; Flannery, B. P.; Teukolsky, S. A.; Vetterling, W. T. *Numerical Recipes in C*; Cambridge University Press: Cambridge, U.K., 1988.
(48) Lundström, P.; Teilum, K.; Carstensen, T.; Bezsonova, I.; Wiesner, S.; Hansen, D. F.; Religa, T. L.; Akke, M.; Kay, L. E. *J. Biomol. NMR* **2007**, *38*, 199−212.
(49) Sattler, M.; Schleucher, J.; Griesinger, C. *Prog. Nucl. Magn. Reson. Spectrosc.* **1999**, *34*, 93−158.
(50) Mulder, F. A. A.; Skrynnikov, N. R.; Hon, B.; Dahlquist, F. W.; Kay, L. E. *J. Am. Chem. Soc.* **2001**, *123*, 967−975.
(51) Hansen, D. F.; Vallurupalli, P.; Kay, L. E. *J. Phys. Chem. B* **2008**, *112*, 5898−5904.
(52) Ishima, R.; Torchia, D. A. *J. Biomol. NMR* **2003**, *25*, 243−248.
(53) Vallurupalli, P.; Hansen, D. F.; Lundström, P.; Kay, L. E. *J. Biomol. NMR* **2009**, *45*, 45−55.
(54) Lundström, P.; Hansen, D. F.; Kay, L. E. *J. Biomol. NMR* **2008**, *42*, 35−47.
(55) Lundström, P.; Vallurupalli, P.; Religa, T. L.; Dahlquist, F. W.; Kay, L. E. *J. Biomol. NMR* **2007**, *38*, 79−88.
(56) Skrynnikov, N. R.; Dahlquist, F. W.; Kay, L. E. *J. Am. Chem. Soc.* **2002**, *124*, 12352−12360.
(57) Orekhov, V. Y.; Korzhnev, D. M.; Kay, L. E. *J. Am. Chem. Soc.* **2004**, *126*, 1886−1891.
(58) Bouvignies, G.; Korzhnev, D. M.; Neudecker, P.; Hansen, D. F.; Cordes, M. H.; Kay, L. E. *J. Biomol. NMR* **2010**, *47*, 135−141.
(59) Hansen, D. F.; Vallurupalli, P.; Lundström, P.; Neudecker, P.; Kay, L. E. *J. Am. Chem. Soc.* **2008**, *130*, 2667−2675.
(60) Delaglio, F.; Grzesiek, S.; Vuister, G. W.; Zhu, G.; Pfeifer, J.; Bax, A. *J. Biomol. NMR* **1995**, *6*, 277−293.
(61) Korzhnev, D. M.; Salvatella, X.; Vendruscolo, M.; Di Nardo, A. A.; Davidson, A. R.; Dobson, C. M.; Kay, L. E. *Nature* **2004**, *430*, 586−590.
(62) Kneller, D.; Kuntz, I. *J. Cell. Biochem.* **1993**, *53*, 254.
(63) Desai, T. M.; Cerminara, M.; Sadqi, M.; Muñoz, V. *J. Biol. Chem.* **2010**, *285*, 34549−34556.
(64) Tamiola, K.; Acar, B.; Mulder, F. A. *J. Am. Chem. Soc.* **2010**, *132*, 18000−18003.